



Article

Supercapacitor Performance of MXene-Coated Carbon Nanofiber Electrodes

Seon Kyung Kim, Seung Ah Kim, Yoon Soo Han and Kyung-Hye Jung *

Department of Advanced Materials and Chemical Engineering, Daegu Catholic University, Gyeongsan 38430, Republic of Korea; seon3193@naver.com (S.K.K.); tmddk554@naver.com (S.A.K.); yshancu@cu.ac.kr (Y.S.H.)

* Correspondence: khjung@cu.ac.kr

Abstract: MXenes consisting of thin layers of transition metal carbides or nitrides are good candidates for electrode materials due to their excellent electrical conductivity and fast ion transfer. Electrospun carbon nanofibers are highly porous and electrically conductive, making them attractive for electrode materials. In this study, free-standing electrodes were prepared by the dip-coating of carbon nanofibers (CNFs) in the MXene (Ti_3C_2) colloidal solution, which was synthesized via the wet-etching of MAX (Ti_3AlC_2) phase, and their chemical structures were investigated by X-ray diffraction and Fourier transform infrared spectroscopy. In addition, scanning and transmission electron microscopy were used to investigate the morphological and crystallographic features of MXene-coated CNFs. Surface area and pore volumes were investigated by nitrogen adsorption/desorption measurements. Supercapacitor performance was studied by assembling a 3-electrode system with 1M aqueous sodium sulfate solution as an electrolyte. MXene-coated CNFs exhibited a maximum specific capacitance of 514 F/g at 0.5 A/g, with energy and power densities of 71.4 Wh/kg at 0.5 A/g and 2.3 kW/kg at 5 A/g, respectively, which are relevantly higher compared to the pristine CNFs due to the pseudocapacitive behavior of MXenes. They also showed comparable cyclic stability during 5000 cycles with the CNFs. This result indicates that MXene-coated carbon nanofibers can be effective electrode materials for electrochemical energy storage.



Citation: Kim, S.K.; Kim, S.A.; Han, Y.S.; Jung, K.-H. Supercapacitor Performance of MXene-Coated Carbon Nanofiber Electrodes. *C* **2024**, *10*, 32. <https://doi.org/10.3390/c10020032>

Academic Editors:
Nikolaos Kostoglou and
Claus Rebholz

Received: 29 December 2023
Revised: 25 March 2024
Accepted: 28 March 2024
Published: 29 March 2024



Copyright: © 2024 by the authors. Licensee MDPI, Basel, Switzerland. This article is an open access article distributed under the terms and conditions of the Creative Commons Attribution (CC BY) license (<https://creativecommons.org/licenses/by/4.0/>).

Keywords: supercapacitors; pseudocapacitors; MXene; polyacrylonitrile; carbon nanofibers

1. Introduction

2D materials have gained the attention of researchers due to their large surface area and superior electrical properties, which makes them promising for use in energy storage devices [1]. Among them, transition metal carbide and/or nitrides, MXenes, have been intensively studied as 2D ceramic materials with a general formula of M_{n+1}X_n , where M represents transition metals and X means carbon and/or nitrogen [2]. They are typically synthesized via wet etching the parent ternary carbides and/or nitrides, MAX phases, using chemical etchants such as hydrofluoric acid (HF) [3]. The general formula of MAX is $\text{M}_{n+1}\text{AX}_n$, with A as an element from the group 13–14 in the periodic table [4]. It is known that MXenes consist of a hexagonal structure, which is similar to their parent MAX phases. MXenes have been explored for use in various fields such as energy storage devices, smart sensors, and electromagnetic shielding systems owing to their excellent hydrophilicity, electrical conductivity, fast ion transfer, and mechanical/chemical stability [5–8]. Carbon and transition metal atoms enable MXenes to exhibit superior pseudocapacitive behavior with good electrical conductivity [9]. In addition, the space between MX layers formed by removing A-layers in MAX phases can accommodate ions such as Li^+ , which makes MXenes very promising for energy storage applications.

Supercapacitors include electrochemical double-layer capacitors (EDLCs) and pseudocapacitors, and display many attractive features including high power and fast charge/discharge

rates, with long cyclic stability [10–12]. Carbon-based EDLCs store their charges electrostatically, which enables the fast and reversible adsorption/desorption of electrolyte ions on the highly porous carbon electrodes [13]. For pseudocapacitors, their energy storage mechanism relies on fast and reversible redox reactions near the surface of the electrode materials, such as conductive polymers or transition metal oxides. They exhibit greater energy density and lower power density compared to EDLCs, since faradaic redox reactions are intrinsically slower than electrosorption. Pseudocapacitance occurs through monolayer ion adsorption with charge transfer and redox reactions on the electrode surface [14]. Therefore, the surface coating of electroactive materials on the porous carbon materials can offer a good strategy to obtain pseudocapacitive performance effectively.

Electrospun carbon nanofibers (CNFs) are good candidates for electrode materials since they exhibit excellent surface porosity and electrical conductivity [15,16]. For synthesis, precursor polymers such as polyacrylonitrile (PAN) or aromatic polyimides are electrospun, activated under air and carbonized under inert gas. It is known that their surface properties and electrochemical performance can be determined by tailoring chemical structures of precursor polymers [17,18]. Electrospinning is known as a facile way to produce composite materials by mixing additives in the polymer solutions. It was reported that MXenes were added to polyvinyl alcohol (PVA) solution and then electrospun to produce MXene-embedded composite nanofibers to improve electrical properties [19]. MXene/CNF composite electrodes prepared by electrospinning and carbonizing MXene flakes in PAN solution were reported for use in supercapacitor electrodes [20–22].

For supercapacitor electrodes, charge storage takes place at the electrode/electrolyte interface, and thus surface properties of electrode materials are critical. Therefore, it is highly required to place redox-active materials such as MXenes on the electrode surface. For the previously reported MXene/CNF composite electrodes, MXenes were embedded inside the fibers, which may not contribute to redox reactions at the electrode/electrolyte interface [20–22]. The surface coating of redox-active materials on the carbon electrode has been achieved by electrodeposition [23,24], hydrothermal deposition [25], chemical grafting [26] or dip-coating [27]. Among them, dip-coating is a facile and cost-effective process to produce composite materials. It was reported that MXene-coated carbon microfibers were prepared via dip-coating for supercapacitor applications, and pre-treatment was conducted prior to dip-coating for better adhesion between MXene flakes and fibers. Dharmasiri et al. reported an electrochemical surface treatment to tailor the surface chemistry of carbon fibers to optimize the adhesion of MXene flakes [28]. In addition, a conductive binder was utilized for the facile adhesion of MXene flakes to carbon fiber surface [29].

This paper reports the preparation of MXene-coated CNFs by dip-coating electrospun CNFs in the MXene colloidal solution without pre-treatment. CNFs are chosen for their EDLC performance with high surface porosity and feasibility as binderless and conductive additive-free electrodes, while MXenes are chosen for their pseudocapacitive charge storage with abundant redox-active sites. Benefiting from these features, MXene-coated CNF electrodes manifest superior energy storage performance.

2. Experimental

For the synthesis of MXenes (Ti_3C_2), titanium aluminum carbide (MAX, Ti_3AlC_2) and dimethyl sulfoxide (DMSO) were purchased from SY innovation (Pyeongtaek, Republic of Korea) and Tokyo-Chemical Industry Co. (TCI, Tokyo, Japan), respectively. Hydrofluoric acid (HF, 48 wt. %) and ammonium hydroxide (NH_4OH) solution were purchased from Sigma-Aldrich Co. (St. Louis, MO, USA). For the synthesis of CNFs, polyacrylonitrile (PAN) and *N,N*-dimethylformamide (DMF) were obtained from Pfaltz & Bauer Inc. (Waterbury, CT, USA) and TCI, respectively. For electrochemical measurements, a 3-electrode set and sodium sulfate (>99.5%, Na_2SO_4) were purchased from Wizmac Co. (Daejeon, Republic of Korea) and TCI, respectively. All chemicals were used as received.

The synthesis of electrospun CNFs was carried out by electrospinning and thermal treatment (oxidative stabilization and the subsequent carbonization) of a precursor polymer,

PAN; 10 wt. % PAN was dissolved in DMF at 40 °C overnight, and then electrospun under a voltage range from 17 to 20 kV. The tip-to-collector distance was 15 cm and the speed of the drum collector was 100 rpm. Electrospun PAN nanofibers were then stabilized at 280 °C at a rate of 2 °C/min for 2 h under air flow and carbonized in 800 °C at a rate of 10 °C/min for 30 min under nitrogen.

To obtain MXene colloidal solution, 0.5 g MAX was added into 10 mL HF for 5 min and stirred for 24 h at room temperature. The solution was then centrifuged for 10 min at 8000 rpm. After centrifugation and washing 6 times, the precipitate was dispersed in 10 mL DMSO followed by sonication for 1 h. After centrifugation for 10 min at 8000 rpm and washing, the precipitate was dispersed in 50 mL distilled water and 5 drops of NH₄OH solution were added while stirring for 30 min. After centrifugation for 10 min at 8000 rpm, a dark supernatant was obtained. MXene-coated CNFs were obtained by dip-coating CNFs in the MXene colloidal solution at 40 °C for 5 h, then vacuum-dried at 60 °C for 12 h. This is represented as M-CNFs.

The surface morphology and elemental compositions of synthesized CNFs and M-CNFs were investigated by scanning electron microscopy (SEM) and energy dispersive X-ray spectroscopy (EDS), respectively, using an SU8220 (Hitachi, Chiyoda, Japan). The crystal structures of MXene and CNFs were determined by X-ray diffraction (XRD, MiniFlex, Rigaku, Japan) scanning from a 2θ range of 3 to 90 degrees at a rate of 5 degrees/min. Attenuated total reflection Fourier transform infrared (ATR-FTIR) spectroscopy was conducted to study their chemical structures on a VERTEX 80 V (Bruker, Bremen, Germany) using a germanium crystal substrate. Microstructures of M-CNFs were characterized with high-resolution transmission electron microscopy (HRTEM, Titan G2 ChemiSTEM Cs Probe, FEI Company, Hillsboro, OR, USA) after sonication in ethanol for 10 min. Surface properties were measured via nitrogen adsorption/desorption isotherms using a surface area analyzer (Belsorp-Max, MicrotracBEL, Osaka, Japan). The specific surface area was computed using the Brunauer–Emmett–Teller (BET) equation.

Supercapacitor performance was measured by assembling a 3-electrode set, which consisted of a Ag/AgCl reference electrode, a platinum counter electrode and 1M Na₂SO₄ aqueous solution as an electrolyte. As a working electrode, synthesized CNFs and M-CNFs were used without the use of any additives such as binders or conductive agents, which result in lower specific capacity. Electrochemical characterization was performed by obtaining cyclic voltammetry (CV) and galvanostatic charge–discharge (GCD) on a WBCS3000S electrochemical work station (Wonatech, Seoul, Republic of Korea). The specific capacitance (C_{sp} , F/g) was calculated by:

$$C_{sp} = \frac{I_d t_d}{mV} \quad (1)$$

where I_d is the discharge current (A), t_d is the discharge time (s), m is the mass of CNFs or M-CNFs (a working electrode (g)), and V is the working potential window (V). In addition, the cycling stability of CNF and M-CNF electrodes was studied by measuring capacitance retention via GCD testing for 5000 cycles. Energy (E , Wh/kg) and power densities (P , kW/kg) were also evaluated via GCD testing by applying Equations (2) and (3), respectively:

$$E = \frac{I_d t_d V}{2m} \quad (2)$$

$$P = \frac{E}{t_d} \quad (3)$$

3. Results and Discussion

Electrospinning and thermal treatment (pre-oxidation and the subsequent carbonization) of PAN dissolved in DMF was carried out to produce CNFs. An MXene/CNFs composite was prepared by dip-coating CNFs in the MXene (Ti₃C₂) colloidal solution synthesized by the HF etching of MAX (Ti₃AlC₂).

The microscopic structure and crystalline nature were investigated by XRD measurement, as shown in Figure 1. The XRD patterns of MAX and MXene are shown in Figure 1a. After HF etching, the strong peak of MAX at $2\theta = 38.8^\circ$ corresponding to the (104) plane obviously decreased, and a non-basal diffraction peak at 60.8° corresponding to the (110) plane appeared, confirming that a part of MAX reacted with HF to form MXene [30]. It is also noticeable that the shift of the reflection peak (002) from 9.7° for MAX to 9.3° for MXenes indicates an increase in the d-spacing due to successful exfoliation by the etching of MAX phases in HF.

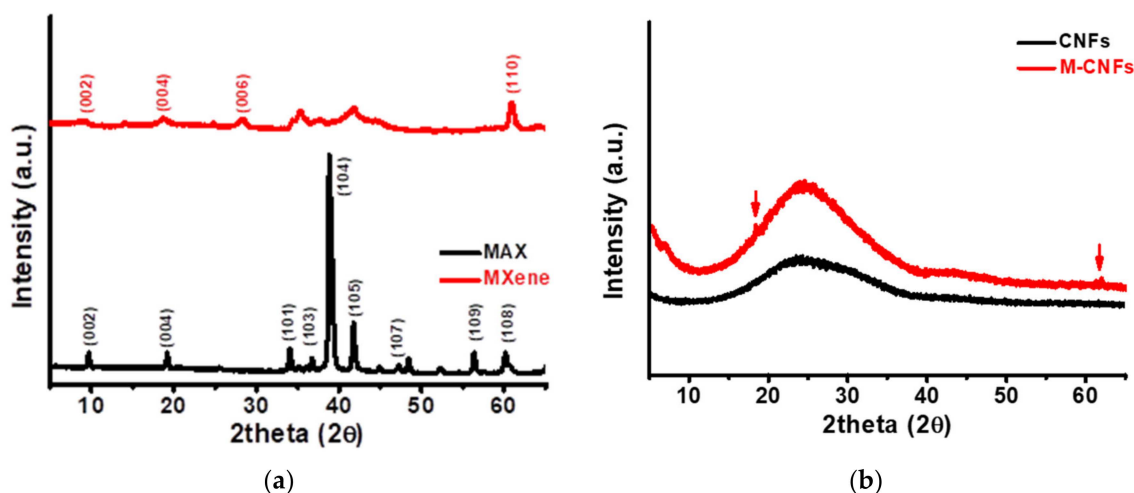


Figure 1. XRD patterns of (a) MAX and MXene phases and (b) CNFs and M-CNFs.

Figure 1b displays the XRD patterns of CNFs and M-CNFs, and both exhibit a significant peak at 24.3° , indicating the formation of a graphite structure via the carbonization of PAN [31]. Different from CNFs, M-CNFs exhibit peaks at 18.4° and 61.7° (indicated by arrows) corresponding to the (004) and (110) plane of MXene, respectively, indicating the presence of MXenes in M-CNFs.

The chemical structures of CNFs and M-CNFs were characterized by FTIR analysis. As illustrated in Figure 2, the absorption peaks of C=C double bond and C–C single bond around 1550 cm^{-1} and 1130 cm^{-1} (indicated by black arrows) appeared in the spectra for both CNFs and M-CNFs. A peak at 535 cm^{-1} (indicated by a red arrow) corresponding to the bending vibration of Ti–O was seen for M-CNFs, while it was not found for CNFs. Indicative peaks of MXenes were clearly found in both the XRD pattern and FTIR spectrum of M-CNFs, which confirms that MXenes were well attached on the CNFs by the dip-coating method.

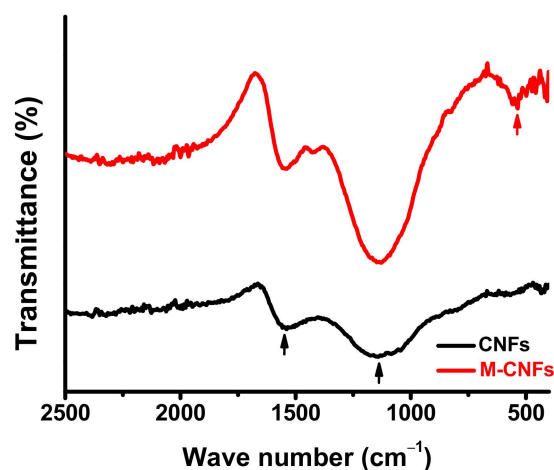


Figure 2. FTIR spectra of CNFs and M-CNFs.

The morphological structures of CNFs and M-CNFs were observed by SEM, as displayed in Figure 3. The successful fabrication of nanofibrous carbon structures through thermal treatment is confirmed by Figure 3a. Figure 3b shows the surface image of M-CNFs, and it is seen that MXenes were well placed on the CNF surface by the dip-coating of CNFs in the MXene colloidal solution. Figure 3c presents a low-magnification SEM image of M-CNFs, where MXene flakes are uniformly dispersed over the surface of dip-coated CNFs. Aqueous colloidal solutions of MXenes were used for dip-coating, since it is well-known that MXenes exhibit high dispersion stability in aqueous media due to their strong hydrophilicity [32,33]. It is also known that oxygen-containing functional groups exist on the CNF surface, resulting from the oxidative stabilization process [34]. As a result of the physisorption caused by these surface features of MXenes and CNFs, the stable dispersion of MXenes over the CNF surface was obtained. In Figure 3d, elementary analysis was carried out by using the EDS, which identified carbon and titanium as the elemental components in M-CNFs. This indicates that carbon is uniformly dispersed throughout the CNF mat, and titanium is clearly found in MXenes.

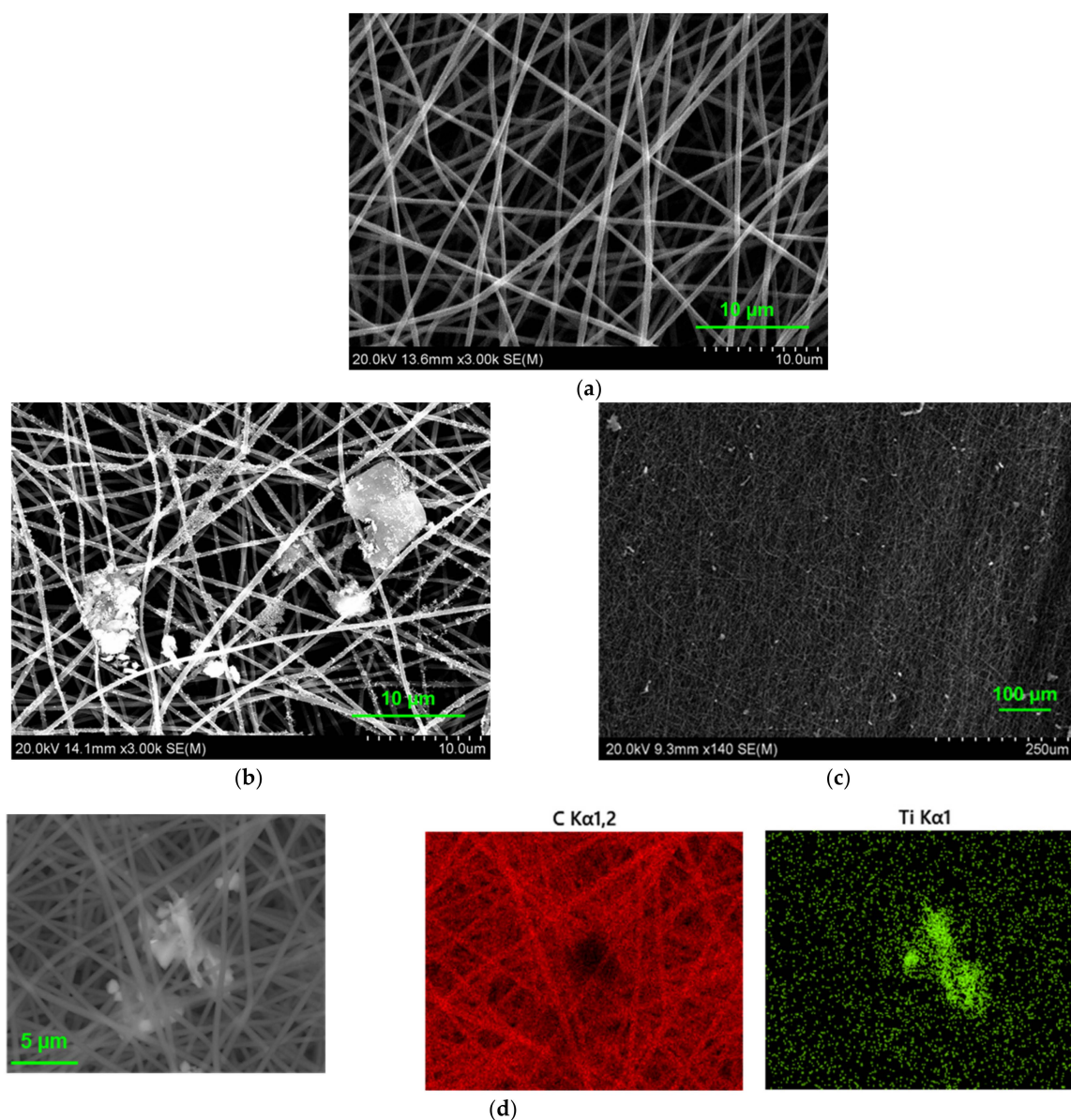


Figure 3. SEM images of (a) CNFs, (b) M-CNFs, (c) M-CNFs (low-magnification) and (d) EDS mapping images of M-CNFs.

To further observe microstructures, synthesized MXenes and M-CNFs were characterized by TEM, as displayed in Figure 4. A 2D nanosheet of the synthesized MXene is seen in Figure 4a, which confirms the successful exfoliation of MAX phases via HF etching. The higher-magnification image shows that the thickness of a single layer of MXene was 0.922 nm, which is consistent with the literature [35,36]. Figure 4b shows a TEM image of M-CNFs, and it is clearly seen that the MXene flake was attached to the surface of a single fiber.

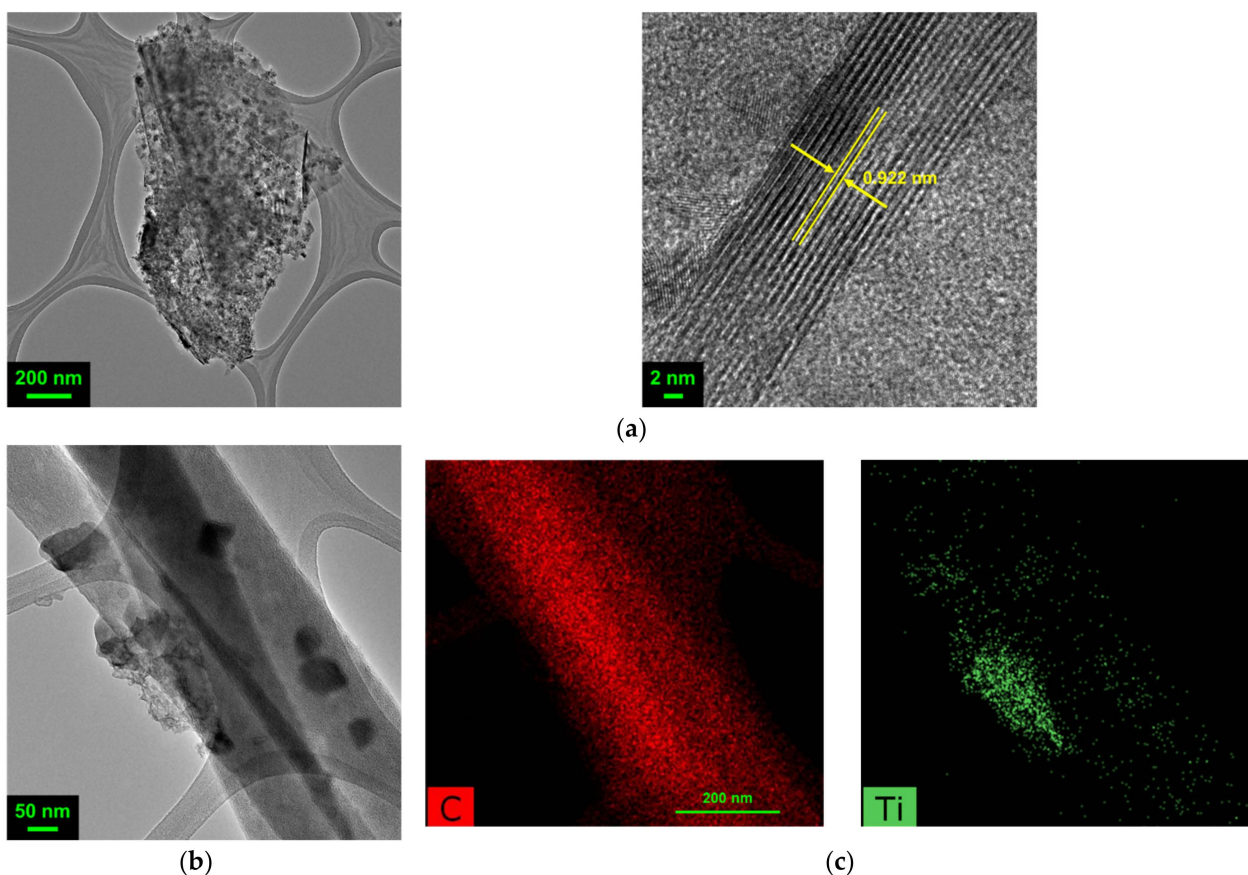


Figure 4. HR TEM images of (a) MXene and (b) M-CNFs, and (c) EDS mapping images of M-CNFs.

The surface properties of synthesized CNFs and M-CNFs were investigated by measuring the nitrogen adsorption and desorption isotherms, as presented in Figure 5. The isotherms for both CNFs and M-CNFs show a type I behavior, which is typically observed in microporous materials. The surface and pore characteristics are shown in Table 1. The CNFs synthesized via thermal treatment (oxidative stabilization and carbonization) of electrospun PAN showed a high specific surface area of $891.46 \text{ m}^2/\text{g}$, with a total pore volume of $0.415 \text{ cm}^3/\text{g}$. After dip-coating CNFs in the MXene colloidal solution, the surface area and pore volumes were decreased, since MXene flakes were placed on the surfaces of highly porous CNFs, which may have contributed surface-induced pseudocapacitance, and the pores of CNFs were covered by some MXene flakes larger than the fiber diameters of CNFs, as seen in Figure 3b,c. Still, M-CNFs displayed a high specific surface area of $663.03 \text{ m}^2/\text{g}$ with a total pore volume of $0.283 \text{ cm}^3/\text{g}$. It was also found that the proportions of meso-pores in the pore diameter range of 2–50 nm for both CNFs and M-CNFs were around 10%.

The pseudocapacitive performance was investigated by assembling a three-electrode cell with Ag/AgCl and a Pt plate as the reference electrode and counter electrode, respectively, and with $1 \text{ M Na}_2\text{SO}_4$ aqueous solution as an electrolyte. Synthesized CNFs and M-CNFs were applied as a binder and conductive agent-free working electrode. Figure 6 shows CV curves taken at various scanning rates ranging from 10 to 100 mV/s . The current

densities of both CNFs and M-CNFs reduced as the scan rate was increased, since the interaction between the electrode surfaces and the electrolyte ions was limited by kinetic and mass transport parameters [37]. It is apparently demonstrated here that M-CNF electrodes exhibit larger current densities compared to CNFs in the whole range of applied voltages.

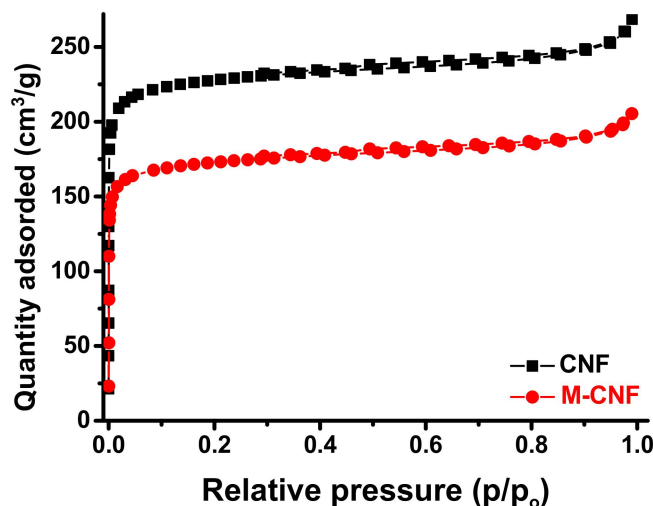


Figure 5. Nitrogen adsorption/desorption isotherms.

Table 1. Structural parameters of CNFs and M-CNFs.

	SSA ¹ (m ² /g)	TPV ² (cm ³ /g)	V _{micro} ³ (cm ³ /g)	V _{meso} ⁴ (cm ³ /g)
CNFs	891.46	0.415	0.372	0.043
M-CNFs	663.03	0.317	0.283	0.034

¹ SSA: specific surface area. ² TPV: total pore volume. ³ V_{micro}: micro-pore (<2 nm) volume. ⁴ V_{meso}: meso-pore (2–50 nm) volume.

Figure 6c displays CV curves of CNF and M-CNF electrodes at a scan rate of 10 mV/s for comparison. The CV curves of untreated CNFs are rectangular, without clear redox peaks, indicating typical EDLC characteristics due to the potential-independent capacitance, while the CV curve for M-CNFs is quasi-rectangular with a shallow hump [38]. The higher capacitive behavior of M-CNFs, which is presented by the larger integrated area of CVs in Figure 6, originates from the pseudocapacitive charge storage induced by MXenes.

Energy performance was further investigated by carrying out galvanostatic charge–discharge testing, as seen in Figure 7a,b, under a current density from 0.5 to 5 A/g and potential range from 0 to 1 V. It is shown that M-CNF electrodes exhibited a significantly longer discharge time (1020 s) compared to that of the CNF electrodes (257 s) at 0.5 A/g. Figure 7c displays a Ragone plot, which presents energy density versus power density at different discharge rates. It can be seen that M-CNFs showed significantly higher energy and power densities at each discharge current density. Table 2 lists electrochemical properties, including maximum specific capacitance (C_{sp}) and energy and power densities (E and P , respectively), computed from the discharge curves in Figure 7. The specific capacitances of CNF and M-CNF electrodes are 130 and 514 F/g, respectively, at 0.5 A/g. It is also noted that the energy densities of CNF and M-CNF electrodes were 18.0 and 71.4 Wh/kg, respectively, at 0.5 A/g. Power density was estimated by an IR drop, which is the abrupt drop in potential at the beginning of discharge, and M-CNFs exhibited a higher value of 2.3 kW/kg at 5 A/g, compared to that of CNFs (1.7 kW/kg). This is attributed to the lower resistance of electrolytes and ion diffusion due to the presence of electrically conductive MXenes.

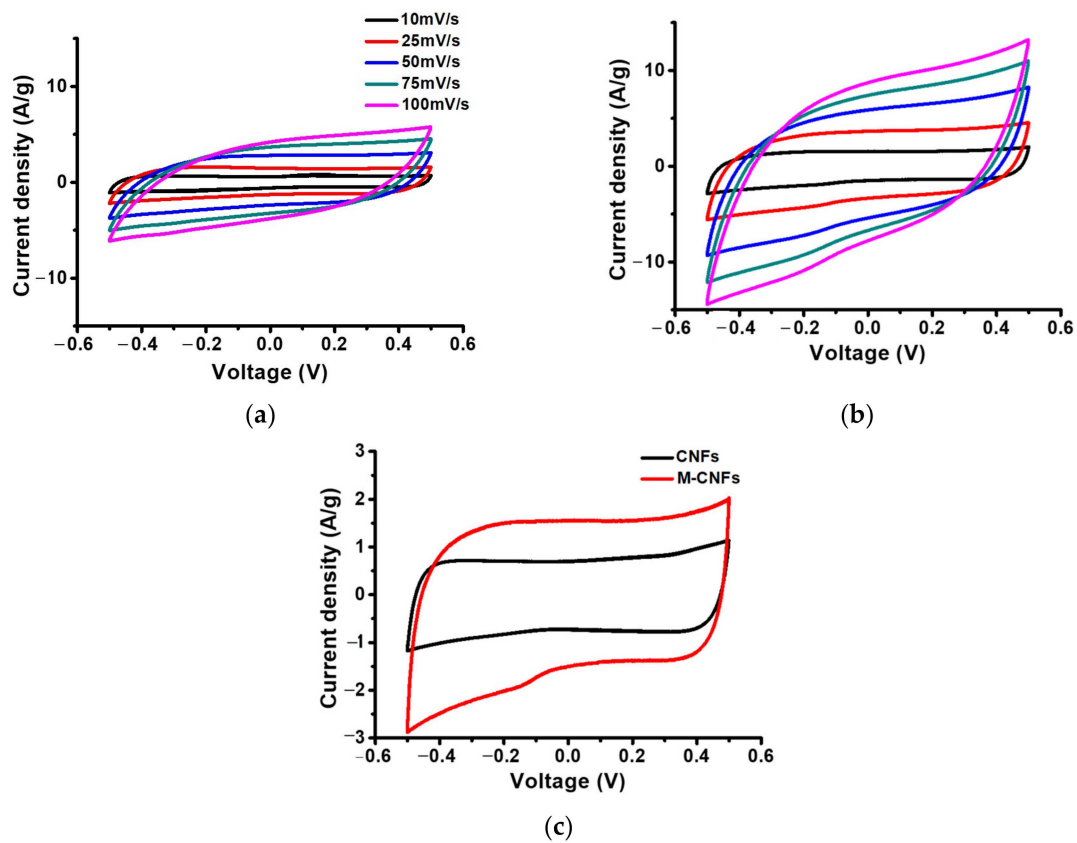


Figure 6. Cyclic voltammograms of (a) CNF, (b) M-CNF electrodes and (c) the comparison at a scan rate of 10 mV/s.

Table 2. Energy storage performance of CNFs and M-CNFs.

Sample	C_{sp} (F/g) @ 0.5 A/g	P (kW/Kg) @ 5 A/g	E (Wh/Kg) @ 0.5 A/g
CNFs	129.5	1.7	17.3
M-CNFs	514.0	2.3	70.1

The discharge curves of M-CNFs show inflection points, and this quasi-linear relationship between the potential and the time indicates pseudocapacitive behavior, which is consistent with CV curves [38]. The higher energy storage performance of M-CNFs is caused by the redox capacitance involving the electrochemical adsorption of ions at the surface of MXenes with a concomitant charge transfer [39].

The cyclic stability of CNF and M-CNF electrodes was investigated by measuring capacitance retention, and specific capacitance values under a current density of 1 A/g were collected for every 250 cycles by GCD testing, as displayed in Figure 8. Untreated CNFs showed slightly higher capacitance retention compared to M-CNFs. Due to the pseudocapacitive behavior of MXenes, M-CNFs showed greater capacitances and energy densities, originating from faradaic redox reactions at the interface between electrodes and electrolytes. This also resulted in lower cyclic stability. However, M-CNFs showed a capacitance retention of 90.7% after 5000 cycles, which is as high as that of untreated CNFs. The superior cyclic stability of both CNF and M-CNF electrodes can be confirmed by the high degree of reversibility. In addition, the electrochemical stability of M-CNF composite electrodes indicates the good attachment of MXenes on the CNF surface while GDC cycling test was performed for 5000 cycles.

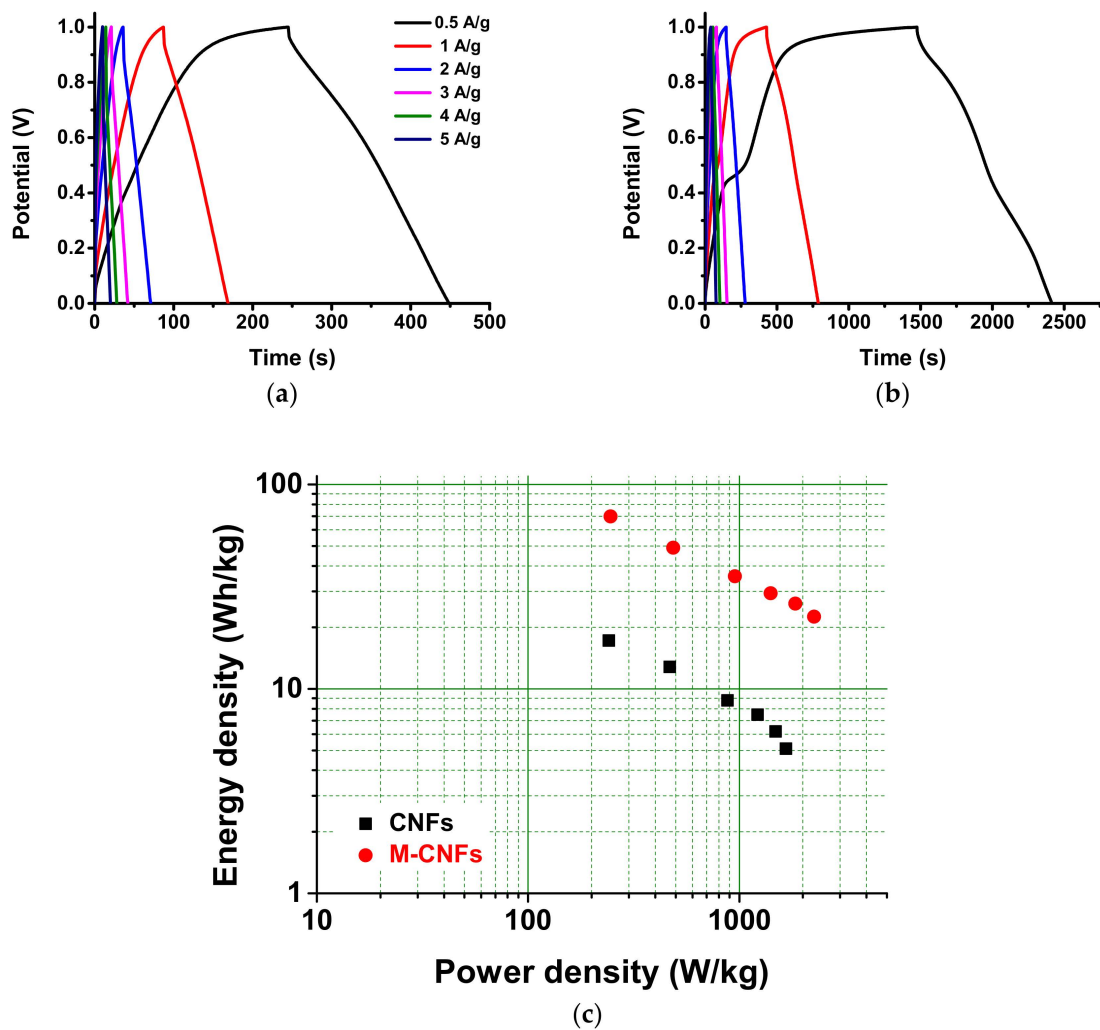


Figure 7. Charge–discharge curves of (a) CNF and (b) M-CNF electrodes, and (c) Ragone plot.

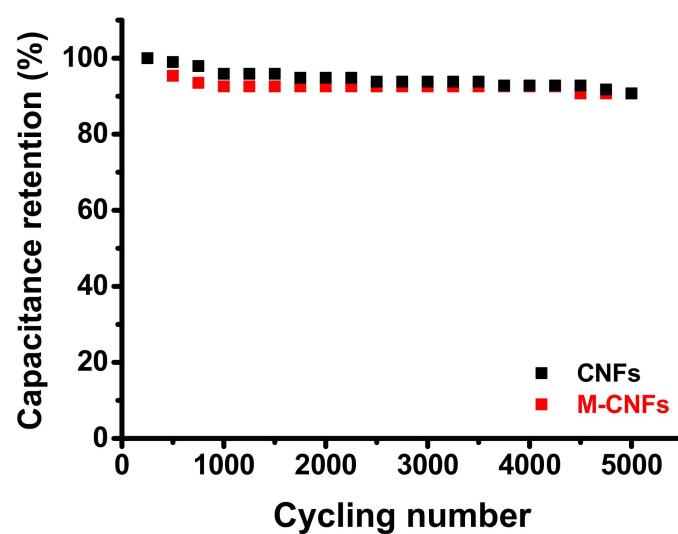


Figure 8. Cyclic stability of CNF and M-CNF electrodes.

MXene/carbon composites have been investigated since they exhibit superior electrochemical properties, owing to the pseudocapacitive behavior of MXenes and the high surface porosity of carbon. It is known that the high stacking of MXenes leads to prolonged

ion transport pathways, resulting in limited energy storage performance, and carbon may effectively enlarge interlayer distances [40]. Li et al. reported the synthesis of graphene (rGO)/carbon nanotube (CNT) nanocomposites as supercapacitor electrodes to achieve compact structures with abundant ions access and fast charge transport [41]. These composite electrodes exhibited ultrahigh volumetric capacitances with high cyclic stability due to the surface redox reactions at the interlayer between the intercalated protons and the oxygen-containing functional groups. It was reported that MXene-bonded activated carbon was synthesized by encapsulating activated carbon at the interlayer of MXene, which resulted in enlarging the interlayer spacing between MXene layers and improving energy storage performance [42]. MXene/graphene composite films were electrostatically assembled using negatively charged MXene and positively charged graphene for ultrafast supercapacitors [43].

MXene-based composites using carbon fibers are a promising approach to developing flexible free-standing electrodes without the use of binders, which can cause poor adhesion, the agglomeration of active materials, excess mass of binders, and low conductivity. Wang et al. fabricated flexible yarn electrodes by biscrolling MXene with CNTs exhibiting superior specific capacitances, and energy and power densities [44]. Hu et al. reported the fabrication of MXene-coated carbon cloth by drop-casting for wearable smart electronics [45]. The M-CNFs used in this study also represent a great candidate for flexible free-standing electrodes showing superior energy storage performance.

Table 3 shows a comparison of the energy storage performances of the composite electrodes of MXenes and carbon in the literature. The specific capacitance of MXene-coated CNF electrodes in this work is higher than that of previously reported electrode materials.

Table 3. Comparison of energy storage performances of MXene/carbon composite electrodes in the literature.

Electrodes	Electrolyte	Scan Rate or Current Density	Specific Capacitance	Reference
MXene/rHGO	3M H ₂ SO ₄	2 mV/s	438 F/g	[46]
MXene/rGO	3M H ₂ SO ₄	2 mV/s	335.4 F/g	[43]
MXene/rGO	PVA/H ₃ PO ₄	10 mV/s	327.5 F/g	[47]
MXene/CNTs	1M MgSO ₄	2 mV/s	390 F/cm ³	[48]
MXene/CFs	1M H ₂ SO ₄	5 mV/s	157 F/g	[28]
MXene/AC	1M Et ₄ NBF ₄ /AN	0.1 A/g	138 F/g	[42]
MXene/CNFs	1M H ₂ SO ₄	50 mV/s	205 mF/cm ²	[20]
MXene/CNFs	1M H ₂ SO ₄	2 mV/s	120 F/g	[21]
MXene/CNFs	3M KOH	1 A/g	249 F/g	[22]
M-CNFs	1M Na ₂ SO ₄	0.5 A/g	514.0 F/g	This work

Composite electrodes of MXene and CNFs that were reported previously were prepared by adding MXene flakes in the precursor polymer solution prior to thermal treatment. Levitt et al. prepared MXene/CNF composite electrodes, of which the specific capacitance was 2.3 times higher than that of CNFs [20]. Hwang et al. also reported the preparation of MXene/CNF electrodes, and their specific capacitance was 3 times higher than that of pure CNFs [21]. The specific capacitance of M-CNFs in this work was 514.0 F/g, which is almost 4 times higher than that of untreated CNFs. This may be because highly conductive MXenes were placed on the surface of highly porous CNFs, which facilitated the access of electrolyte ions to the electrodes.

4. Conclusions

Supercapacitor performance is determined by the energy storage mechanism, which is mainly affected by applied electrode materials. To induce pseudocapacitive behavior driven by faradaic redox reactions at the interface between electrodes and the electrolyte, it is inevitable that the redox-active materials will be placed on the electrode surface. CNFs

were chosen due to their high surface porosity with excellent EDLC performance, and the surfaces of CNFs were coated with MXene phases, which is a well-known redox-active component used to produce electrode materials with surface-induced pseudocapacitance.

In summary, the synthesis, characterization and electrochemical properties of MXene/CNF composites were conducted. They were synthesized by the dip-coating of CNFs prepared from the electrospinning and thermal treatment of PAN in the MXene colloidal solution, which was synthesized by the HF etching of MAX phase. The successful synthesis of an MXene/CNF composite was confirmed by investigating XRD and FTIR spectra, and SEM-EDS. Surface properties were observed via nitrogen adsorption/desorption, and M-CNFs displayed slightly lower surface area and pore volumes. Energy storage performance was measured using a three-electrode cell with Na₂SO₄ as an electrolyte, and M-CNF electrodes showed significantly superior supercapacitor performance, including specific capacitance (514 F/g) and energy and power densities (71.4 Wh/kg and 2.3 kW/kg, respectively), at 0.5 A/g, confirming them as promising electrode materials for supercapacitors.

Author Contributions: Methodology, S.K.K., S.A.K. and Y.S.H.; Validation, S.K.K. and S.A.K.; Formal analysis, S.K.K. and S.A.K.; Investigation, S.K.K.; Writing—original draft, K.-H.J.; Supervision, K.-H.J. All authors have read and agreed to the published version of the manuscript.

Funding: This work was financially supported by Daegu Catholic University (20211044).

Data Availability Statement: Data are contained within the article.

Conflicts of Interest: The authors declare no conflict of interest.

References

1. Kumbhakar, P.; Jayan, J.S.; Madhavikutty, A.S.; Sreeram, P.; Appukuttan, S.; Ito, T.; Tiwary, C.S. Prospective applications of two-dimensional materials beyond laboratory frontiers: A review. *IScience* **2023**, *26*, 106671. [[CrossRef](#)] [[PubMed](#)]
2. Naguib, M.; Kurtoglu, M.; Presser, V.; Lu, J.; Niu, J.; Heon, M.; Hultman, L.; Gogotsi, Y.; Barsoum, M.W. Two-dimensional nanocrystals produced by exfoliation of Ti₃AlC₂. *Adv. Mater.* **2011**, *23*, 4248–4253. [[CrossRef](#)]
3. Alhabeab, M.; Maleski, K.; Anasori, B.; Lelyukh, P.; Clark, L.; Sin, S.; Gogotsi, Y. Guidelines for synthesis and processing of two-dimensional titanium carbide (Ti₃C₂T_x MXene). *Chem. Mater.* **2017**, *29*, 7633–7644. [[CrossRef](#)]
4. Barsoum, M.W. *MAX Phases: Properties of Machinable Ternary Carbides and Nitrides*; John Wiley & Sons: Hoboken, NJ, USA, 2013.
5. Champagne, A.; Charlier, J.-C. Physical properties of 2D MXenes: From a theoretical perspective. *J. Phys. Mater.* **2020**, *3*, 032006. [[CrossRef](#)]
6. Thakur, N.; Kumar, P.; Sati, D.C.; Neffati, R.; Sharma, P. Recent advances in two-dimensional MXenes for power and smart energy systems. *J. Energy Storage* **2022**, *50*, 104604. [[CrossRef](#)]
7. Ho, D.H.; Choi, Y.Y.; Jo, S.B.; Myoung, J.M.; Cho, J.H. Sensing with MXenes: Progress and prospects. *Adv. Mater.* **2021**, *33*, 2005846. [[CrossRef](#)] [[PubMed](#)]
8. Iqbal, A.; Sambyal, P.; Koo, C.M. 2D MXenes for electromagnetic shielding: A review. *Adv. Funct. Mater.* **2020**, *30*, 2000883. [[CrossRef](#)]
9. Xu, X.; Yang, L.; Zheng, W.; Zhang, H.; Wu, F.; Tian, Z.; Zhang, P.; Sun, Z. MXenes with applications in supercapacitors and secondary batteries: A comprehensive review. *Mater. Rep. Energy* **2022**, *2*, 100080. [[CrossRef](#)]
10. Trasatti, S.; Kurzweil, P. Electrochemical supercapacitors as versatile energy stores. *Platin. Met. Rev.* **1994**, *38*, 46–56. [[CrossRef](#)]
11. Halper, M.S.; Ellenbogen, J.C. *Supercapacitors: A Brief Overview*; The MITRE Corporation: McLean, VA, USA, 2006; Volume 1.
12. Yu, A.; Chabot, V.; Zhang, J. *Electrochemical Supercapacitors for Energy Storage and Delivery: Fundamentals and Applications*; Taylor & Francis: Abingdon, UK, 2013.
13. Pandolfo, A.G.; Hollenkamp, A.F. Carbon properties and their role in supercapacitors. *J. Power Sources* **2006**, *157*, 11–27. [[CrossRef](#)]
14. Wang, X.; Kajiyama, S.; Iinuma, H.; Hosono, E.; Oro, S.; Moriguchi, I.; Okubo, M.; Yamada, A. Pseudocapacitance of MXene nanosheets for high-power sodium-ion hybrid capacitors. *Nat. Commun.* **2015**, *6*, 6544. [[CrossRef](#)] [[PubMed](#)]
15. Kim, C. Electrochemical characterization of electrospun activated carbon nanofibres as an electrode in supercapacitors. *J. Power Sources* **2005**, *142*, 382–388. [[CrossRef](#)]
16. Zhang, B.; Kang, F.; Tarascon, J.-M.; Kim, J.-K. Recent advances in electrospun carbon nanofibers and their application in electrochemical energy storage. *Prog. Mater. Sci.* **2016**, *76*, 319–380. [[CrossRef](#)]
17. Kim, S.J.; Son, Y.J.; Jeon, B.; Han, Y.S.; Kim, Y.-J.; Jung, K.-H. Surface crosslinking of 6FDA-durene nanofibers for porous carbon nanofiber electrodes in electrochemical double layer capacitors. *Nanotechnology* **2020**, *31*, 215404. [[CrossRef](#)]
18. Lee, D.G.; Lee, B.C.; Jung, K.-H. Preparation of Porous Carbon Nanofiber Electrodes Derived from 6FDA-Durene/PVDF Blends and Their Electrochemical Properties. *Polymers* **2021**, *13*, 720. [[CrossRef](#)] [[PubMed](#)]

19. Sobolčiak, P.; Ali, A.; Hassan, M.K.; Helal, M.I.; Tanvir, A.; Popelka, A.; Al-Maadeed, M.A.; Krupa, I.; Mahmoud, K.A. 2D Ti₃C₂Tx (MXene)-reinforced polyvinyl alcohol (PVA) nanofibers with enhanced mechanical and electrical properties. *PLoS ONE* **2017**, *12*, e0183705. [[CrossRef](#)] [[PubMed](#)]
20. Levitt, A.S.; Alhabeab, M.; Hatter, C.B.; Sarycheva, A.; Dion, G.; Gogotsi, Y. Electrospun MXene/carbon nanofibers as supercapacitor electrodes. *J. Mater. Chem. A* **2019**, *7*, 269–277. [[CrossRef](#)]
21. Hwang, H.; Byun, S.; Yuk, S.; Kim, S.; Song, S.H.; Lee, D. High-rate electrospun Ti₃C₂Tx MXene/carbon nanofiber electrodes for flexible supercapacitors. *Appl. Surf. Sci.* **2021**, *556*, 149710. [[CrossRef](#)]
22. Yan, S.-x.; Luo, S.-h.; Wang, Q.; Zhang, Y.-h.; Liu, X. Rational design of hierarchically sulfide and MXene-reinforced porous carbon nanofibers as advanced electrode for high energy density flexible supercapacitors. *Compos. B Eng.* **2021**, *224*, 109246. [[CrossRef](#)]
23. Dirican, M.; Yanilmaz, M.; Fu, K.; Lu, Y.; Kizil, H.; Zhang, X. Carbon-enhanced electrodeposited SnO₂/carbon nanofiber composites as anode for lithium-ion batteries. *J. Power Sources* **2014**, *264*, 240–247. [[CrossRef](#)]
24. Liu, Y.; Lu, Q.; Huang, Z.; Sun, S.; Yu, B.; Evariste, U.; Jiang, G.; Yao, J. Electrodeposition of Ni-Co-S nanosheet arrays on N-doped porous carbon nanofibers for flexible asymmetric supercapacitors. *J. Alloys Compd.* **2018**, *762*, 301–311. [[CrossRef](#)]
25. Wang, H.; Deng, J.; Chen, Y.; Xu, F.; Wei, Z.; Wang, Y. Hydrothermal synthesis of manganese oxide encapsulated multiporous carbon nanofibers for supercapacitors. *Nano Res.* **2016**, *9*, 2672–2680. [[CrossRef](#)]
26. Kotal, M.; Thakur, A.K.; Bhowmick, A.K. Polyaniline–carbon nanofiber composite by a chemical grafting approach and its supercapacitor application. *ACS Appl. Mater. Interfaces* **2013**, *5*, 8374–8386. [[CrossRef](#)] [[PubMed](#)]
27. Paleo, A.J.; Staiti, P.; Brigandi, A.; Ferreira, F.; Rocha, A.; Lufrano, F. Supercapacitors based on AC/MnO₂ deposited onto dip-coated carbon nanofiber cotton fabric electrodes. *Energy Storage Mater.* **2018**, *12*, 204–215. [[CrossRef](#)]
28. Dharmasiri, B.; Usman, K.A.S.; Qin, S.A.; Razal, J.M.; Tran, N.T.; Coia, P.; Harte, T.; Henderson, L.C. Ti₃C₂Tx MXene coated carbon fibre electrodes for high performance structural supercapacitors. *Chem. Eng. J.* **2023**, *476*, 146739. [[CrossRef](#)]
29. Zhang, J.; Seyedin, S.; Gu, Z.; Yang, W.; Wang, X.; Razal, J.M. MXene: A potential candidate for yarn supercapacitors. *Nanoscale* **2017**, *9*, 18604–18608. [[CrossRef](#)] [[PubMed](#)]
30. Ghosh, A.; Pal, H.; Das, T.; Chatterjee, S.; Das, A. Synthesis and Characterization of MXene from MAX phase. *Mater. Today Proc.* **2022**, *58*, 714–716. [[CrossRef](#)]
31. Gupta, A.; Paliwal, D.; Bajaj, P. Acrylic precursors for carbon fibers. *J. Polym. Sci. Part. D Macromol. Rev.* **1991**, *31*, 1–89. [[CrossRef](#)]
32. Rozmysłowska, A.; Wojciechowski, T.; Ziemkowska, W.; Chlubny, L.; Olszyna, A.; Poźniak, S.; Tomkiewicz, K.; Jastrzębska, A. Colloidal properties and stability of 2D Ti₃C₂ and Ti₂C MXenes in water. *Int. J. Electrochem. Sci.* **2018**, *13*, 10837–10847. [[CrossRef](#)]
33. Maleski, K.; Mochalin, V.N.; Gogotsi, Y. Dispersions of two-dimensional titanium carbide MXene in organic solvents. *Chem. Mater.* **2017**, *29*, 1632–1640. [[CrossRef](#)]
34. Wu, M.; Wang, Q.; Li, K.; Wu, Y.; Liu, H. Optimization of stabilization conditions for electrospun polyacrylonitrile nanofibers. *Polym. Degrad. Stab.* **2012**, *97*, 1511–1519. [[CrossRef](#)]
35. Yuen, A.C.Y.; Chen, T.B.Y.; Lin, B.; Yang, W.; Kabir, I.I.; Cordeiro, I.M.D.C.; Whitten, A.E.; Mata, J.; Yu, B.; Lu, H.-D. Study of structure morphology and layer thickness of Ti₃C₂ MXene with Small-Angle Neutron Scattering (SANS). *Compos. C Open Access* **2021**, *5*, 100155. [[CrossRef](#)]
36. Rahman, U.U.; Humayun, M.; Ghani, U.; Usman, M.; Ullah, H.; Khan, A.; El-Metwaly, N.M.; Khan, A. MXenes as emerging materials: Synthesis, properties, and applications. *Molecules* **2022**, *27*, 4909. [[CrossRef](#)]
37. Hashemi, M.; Rahmanifar, M.S.; El-Kady, M.F.; Noori, A.; Mousavi, M.F.; Kaner, R.B. The use of an electrocatalytic redox electrolyte for pushing the energy density boundary of a flexible polyaniline electrode to a new limit. *Nano Energy* **2018**, *44*, 489–498. [[CrossRef](#)]
38. Jiang, Y.; Liu, J. Definitions of pseudocapacitive materials: A brief review. *Energy Environ. Mater.* **2019**, *2*, 30–37. [[CrossRef](#)]
39. Kumar, S.; Rehman, M.A.; Lee, S.; Kim, M.; Hong, H.; Park, J.-Y.; Seo, Y. Supercapacitors based on Ti₃C₂Tx MXene extracted from supernatant and current collectors passivated by CVD-graphene. *Sci. Rep.* **2021**, *11*, 649. [[CrossRef](#)] [[PubMed](#)]
40. Zhu, Y.; Rajoua, K.; Le Vot, S.; Fontaine, O.; Simon, P.; Favier, F. Modifications of MXene layers for supercapacitors. *Nano Energy* **2020**, *73*, 104734. [[CrossRef](#)]
41. Li, K.; Wang, X.; Wang, X.; Liang, M.; Nicolosi, V.; Xu, Y.; Gogotsi, Y. All-pseudocapacitive asymmetric MXene-carbon-conducting polymer supercapacitors. *Nano Energy* **2020**, *75*, 104971. [[CrossRef](#)]
42. Yu, L.; Hu, L.; Anasori, B.; Liu, Y.-T.; Zhu, Q.; Zhang, P.; Gogotsi, Y.; Xu, B. MXene-bonded activated carbon as a flexible electrode for high-performance supercapacitors. *ACS Energy Lett.* **2018**, *3*, 1597–1603. [[CrossRef](#)]
43. Yan, J.; Ren, C.E.; Maleski, K.; Hatter, C.B.; Anasori, B.; Urbankowski, P.; Sarycheva, A.; Gogotsi, Y. Flexible MXene/graphene films for ultrafast supercapacitors with outstanding volumetric capacitance. *Adv. Funct. Mater.* **2017**, *27*, 1701264. [[CrossRef](#)]
44. Wang, Z.; Qin, S.; Seyedin, S.; Zhang, J.; Wang, J.; Levitt, A.; Li, N.; Haines, C.; Ovalle-Robles, R.; Lei, W. High-performance biscrolled MXene/carbon nanotube yarn supercapacitors. *Small* **2018**, *14*, 1802225. [[CrossRef](#)] [[PubMed](#)]
45. Hu, M.; Hu, T.; Cheng, R.; Yang, J.; Cui, C.; Zhang, C.; Wang, X. MXene-coated silk-derived carbon cloth toward flexible electrode for supercapacitor application. *J. Energy Chem.* **2018**, *27*, 161–166. [[CrossRef](#)]
46. Fan, Z.; Wang, Y.; Xie, Z.; Wang, D.; Yuan, Y.; Kang, H.; Su, B.; Cheng, Z.; Liu, Y. Modified MXene/holey graphene films for advanced supercapacitor electrodes with superior energy storage. *Adv. Sci.* **2018**, *5*, 1800750. [[CrossRef](#)] [[PubMed](#)]

47. Yang, Q.; Xu, Z.; Fang, B.; Huang, T.; Cai, S.; Chen, H.; Liu, Y.; Gopalsamy, K.; Gao, W.; Gao, C. MXene/graphene hybrid fibers for high performance flexible supercapacitors. *J. Mater. Chem. A* **2017**, *5*, 22113–22119. [[CrossRef](#)]
48. Zhao, M.-Q.; Ren, C.E.; Ling, Z.; Lukatskaya, M.R.; Zhang, C.; Van Aken, K.L.; Barsoum, M.W.; Gogotsi, Y. Flexible MXene/carbon nanotube composite paper with high volumetric capacitance. *Adv. Mater.* **2014**, *27*, 339–345. [[CrossRef](#)]

Disclaimer/Publisher’s Note: The statements, opinions and data contained in all publications are solely those of the individual author(s) and contributor(s) and not of MDPI and/or the editor(s). MDPI and/or the editor(s) disclaim responsibility for any injury to people or property resulting from any ideas, methods, instructions or products referred to in the content.